Alzheimer's & Dementia 13 (2017) 225-235

Featured Article

Tract-specific white matter hyperintensities disrupt neural network function in Alzheimer's disease

Alexander N. W. Taylor[a], Lana Kambeitz-Ilankovic[b], Benno Gesierich[a], Lee Simon-Vermot[a], Nicolai Franzmeier[a], Miguel Á. Araque Caballero[a], Sophia Müller[c], Liu Hesheng[d], Birgit Ertl-Wagner[c], Katharina Bürger[c], Michael W. Weiner[e,f], Martin Dichgans[a,g], Marco Duering[a], Michael Ewers[a,*], for the Alzheimer's Disease Neuroimaging Initiative (ADNI)

[a]*Institute for Stroke and Dementia Research, Klinikum der Universität München, Ludwig-Maximilians-Universität LMU, Munich, Germany*
[b]*Department of Psychiatry and Psychotherapy, Ludwig-Maximilians-Universität LMU, Munich, Germany*
[c]*Institute of Clinical Radiology, Klinikum der Universität München, Ludwig-Maximilians-Universität LMU, Munich, Germany*
[d]*Athinoula A. Martinos Center for Biomedical Imaging, Department of Radiology, Massachusetts General Hospital, Harvard Medical School, Charlestown, MA, USA*
[e]*Department of Radiology & Biomedical Imaging, University of California, San Francisco, CA, USA*
[f]*VA Medical Center, Center for Imaging of Neurodegenerative Diseases, San Francisco, CA, USA*
[g]*Munich Cluster for Systems Neurology (SyNergy), Munich, Germany*

Abstract

Introduction: White matter hyperintensities (WMHs) increase the risk of Alzheimer's disease (AD). Whether WMHs are associated with the decline of functional neural networks in AD is debated.
Method: Resting-state functional magnetic resonance imaging and WMH were assessed in 78 subjects with increased amyloid levels on AV-45 positron emission tomography (PET) in different clinical stages of AD. We tested the association between WMH volume in major atlas-based fiber tract regions of interest (ROIs) and changes in functional connectivity (FC) between the tracts' projection areas within the default mode network (DMN).
Results: WMH volume within the inferior fronto-occipital fasciculus (IFOF) was the highest among all tract ROIs and associated with reduced FC in IFOF-connected DMN areas, independently of global AV-45 PET. Higher AV-45 PET contributed to reduced FC in IFOF-connected, temporal, and parietal DMN areas.
Conclusions: High fiber tract WMH burden is associated with reduced FC in connected areas, thus adding to the effects of amyloid pathology on neuronal network function.

Keywords: Alzheimer's disease; Functional connectivity; Fiber tract; Resting-state fMRI; White matter hyperintensities; Vascular; Amyloid-beta

1. Introduction

Higher volume of white matter hyperintensities (WMHs) is associated with increased risk of dementia, not only vascular dementia but also Alzheimer's disease (AD)–related dementia [1]. In AD, increased WMH volume

*Corresponding author. Tel.: +49-(0)89440046221; Fax: +49-(0)89440046113.
E-mail address: michael.ewers@med.uni-muenchen.de

http://dx.doi.org/10.1016/j.jalz.2016.06.2358

contributes to cognitive decline independently from abnormally high levels of Aβ in the brain [2]. These studies suggest that WMHs are an important factor that exacerbates the cognitive deficits in AD.

The contribution of WMH to the impairment of functional networks underlying cognitive changes, however, is not well understood. Most studies assessing the effects of WMH on functional brain changes in AD have focused on fluorodeoxyglucose positron emission tomography (FDG-PET) [3–6]. Results from these studies showed that higher global WMH volume, measured within the whole white matter, is associated primarily with prefrontal FDG-PET hypometabolism [6–9]. Higher WMH volume has further been shown to be associated with lower FDG-PET in temporoparietal brain areas in subjects with mild cognitive impairment (MCI) or AD dementia [4]. Such effects of WMH remained when controlling for biomarker levels of Aβ [4,8]. A recent resting-state functional magnetic resonance imaging (rsfMRI) study showed that higher WMH burden is associated with impaired brain function [10]. However, these studies used global measures of WMH volume averaged across the entire white matter [4,6–10] or large brain regions regardless of anatomical boundaries of fiber tracts [11].

Recent studies on ischemic WMH have highlighted the relevance of lesion location and of anatomical connections between WMH and cortical gray matter [12–14]. By studying patients with genetically defined small vessel disease, we recently demonstrated that white matter lesions are associated with local gray matter atrophy specifically in projection areas of the connecting fiber tracts [15]. Applied to AD, we hypothesized that higher WMH volume in anatomically defined white matter tracts is associated with functional brain changes specifically in connected cortical regions.

To test this hypothesis, we measured the effect of WMH and levels of AV-45 positron emission tomography (PET) binding of Aβ on functional connectivity (FC) within the default mode network (DMN), which can be readily identified during rsfMRI in older subjects [16]. We focused on FC changes within the DMN because this is the major functional neural network that shows reduced FC in AD and for which the fiber tract connections between different DMN regions have been demonstrated [17,18]. Specifically, we tested whether WMH in major fiber tract atlas ROIs of the DMN are associated with reduced FC in cortical regions connected by these fiber tracts.

2. Methods

2.1. Subjects

All subjects were recruited within the multicenter network Alzheimer's Disease Neuroimaging Initiative (ADNI, recruitment phases GO and II) [19]. ADNI is a longitudinal study started in 2003 as a public–private partnership to investigate neuroimaging features, neuropsychological parameters, and other biomarker for tracking and predicting AD-related cerebral and cognitive changes [19] (Supplementary Methods 1). Ethical approval was obtained by the ADNI investigators (http://www.adni-info.org/pdfs/adni_protocol_9_19_08.pdf). This study was approved by the institutional review boards of all the participating institutions within ADNI.

AD dementia was diagnosed according to the National Institute of Neurological and Communicative Disorders and Stroke-Alzheimer's Disease and Related Disorders Association (NINCDS-ADRDA) criteria [20], and amnestic MCI (aMCI) was diagnosed according to the Mayo Clinic criteria [21,22] (for details, see Supplementary Methods 2). Subjects were selected by the following criteria: availability of an AV-45 PET scan (to assess levels of Aβ), three-dimensional (3D) T1-weighted magnetic resonance imaging (MRI) scan (for spatial normalization), fluid-attenuated inversion recovery (FLAIR) scan (to assess WMH), and rsfMRI (to assess FC). In addition, MCI and AD dementia patients had to show abnormally high global AV-45 PET binding (Aβ+) as defined by a previously established criterion of gAV-45 PET $>$ 1.11 [23]. The different imaging modalities were acquired no longer than 13 months apart from each other (average delay between AV-45 PET and MRI scans was 20 days, range = −357 to 378 days).

Of the initial sample of N = 138 subjects meeting our criteria, 36 subjects were excluded due to poor signal in rsfMRI as a consequence of atrophy in parietal and frontal regions (N = 18), FLAIR segmentation failures (N = 2), excessive movement artifacts visible in rsfMRI (translations $>$ 3 mm or rotations $>$ 2°) or FLAIR scans (N = 8), or failed spatial normalization (N = 8). Failed spatial normalization resulted from large ventricles that caused an erroneous high-dimensional spatial transformation (for details of spatial normalization, see Section 2.4). The final sample included 102 subjects, that is, 38 cognitively healthy control subjects (HC; Aβ+ n = 14, Aβ− n = 24), 42 subjects with aMCI Aβ+, and 22 patients with AD dementia.

2.2. MRI acquisition

All rsfMRI scans were obtained on Philips 3T MRI scanners, with an eight-channel head coil. Briefly, the rsfMRI scans were acquired using a single-shot T2*-weighted echo-planar imaging pulse sequence with a 3.3-mm slice thickness (repetition time = 3000 ms). The 3D T1-weighted magnetic resonance images were acquired using an magnetization-prepared rapid gradient-echo (MPRAGE) sequence with a spatial resolution of 1 × 1 × 1.2-mm^3 (170 slices). FLAIR scans were obtained with a spatial resolution of 0.86 × 0.86 × 5-mm^3 voxel resolution. Full details of all MRI scanner protocols for T2*-weighted, MPRAGE T1-

weighted, and FLAIR images can be found at http://adni.loni.usc.edu/methods/documents/mri-protocols/.

2.3. AV-45 PET acquisition

AV-45 PET scans were acquired on a variety of different PET scanners (Siemens, GE and Philips). AV-45 PET scans consisted of 4 × 300-second frames measured 50 minutes after injection of 10 ± 1.0 mCi of ^{18}F-Florbetapir AV-45. Global AV-45 PET values (gAV-45 PET) were obtained as an average of the image values within several large ROIs as previously described [23]. Preprocessing of the AV-45 PET scans and computation of the gAV-45 PET values were done centrally by the ADNI core (http://adni.loni.usc.edu/data-samples/pet).

2.4. RsfMRI analysis

Standard preprocessing of rsfMRI images was performed including realignment of images, correction of movement artifacts, and coregistration to native space 3D T1-weighted images. Spatial normalization of the preprocessed data was done through diffeomorphic high-dimensional registration as implemented in the DARTEL toolbox (SPM 8; Wellcome Trust Centre for Neuroimaging, University College London, see Supplementary Methods 3 for details) [24]. Next, the motion parameters and the BOLD signal time courses within the white matter and cerebrospinal fluid (CSF) were regressed out. The BOLD signal was low-pass filtered (<0.1 Hz) and detrended. These preprocessing steps were conducted with the software program Resting-State fMRI Data Analysis Toolkit (REST) [25]. Based on these preprocessed scans in Montreal Neurological Institute (MNI) space (1.5 mm), a groupwise independent component analysis (ICA) was conducted, using the GIFT fMRI Toolbox (version 2.0.b) [26] to extract the DMN component. The global brain signal was removed, and a total of 20 independent components were estimated across subjects, using the Infomax algorithm. Spatial correlation analysis of the group ICA–derived maps versus the independent component map of the DMN reported by Smith et al. [27] showed a high spatial correlation of r = 0.71 for a single-group ICA component. The next best fitting component showed a marked drop to r = 0.29, thus allowing for an unambiguous identification of the DMN.

2.5. WMH segmentation and projection onto fiber tract ROIs

The preprocessing steps involved in the WMH measurement are displayed in Supplementary Fig. 1. WMH was segmented from the whole brain FLAIR images, using a semiautomatic classification procedure. In the first step, FLAIR images were bias-corrected and segmented into three-tissue probability maps using the FAST toolbox [28] from the FMRIB software library [29] (FSL, version v5.0). As a result, for all subjects, WMH and CSF were mixed in the same tissue probability map that was thresholded at a probability >0.3. Given that these two tissue types have nonoverlapping FLAIR intensities distributions (WMH being very bright and CSF very dark), WMH could be unambiguously segregated. This was done using a histogram segmentation based on the Otsu method [30]. Two independent raters manually edited the resulting WMH segmentations to remove clusters that were misclassified as WMH (Supplementary Fig. 2). Manual editing was done using a custom written software tool, developed in MATLAB (R2013b; MathWorks, Natick, MA, USA). The inter-rater reliability of the WMH assessment yielded a Dice coefficient of 0.98.

The resulting WMH maps in native space were then normalized to MNI space (2 mm) by a two-step procedure. First, the FLAIR images were registered (affine) to the MPRAGE T1-weighted images using FSL FLIRT [31]. Second, normalization to MNI space (2 mm) was estimated based on the T1-weighted MRI sequence using linear (FSL FLIRT) and nonlinear (FSL FNIRT) registration with standard parameters. The WMH maps were spatially normalized, by applying the transformation parameters estimated in this two-step procedure. Tract-specific WMH volumes were then calculated by superimposing the spatially normalized WMH maps onto the Johns Hopkins University International Consortium for Brain Mapping probabilistic fiber tract atlas (JHU-ICBM-tracts) [32] in the MNI152 standard space. The atlas was comprised of probability maps for 20 main fiber tracts. In order to calculate the WMH volume for a particular fiber tract, the WMH map was overlaid on the corresponding probability map and used as a mask. The voxel-wise probabilities were then summed up across all voxels within this mask. Finally, the tract-specific WMH volumes were normalized to the tracts' total volumes, calculated as the sum of voxel-wise fiber tract probabilities (from the JHU-ICBM-tracts) throughout the whole brain. This procedure has been described previously [33].

2.6. Mapping DMN regions connected by the atlas-based fiber tract ROIs

The initial set of fiber tracts was based on previous reports of fiber tract connections between DMN brain regions [34–41] and included the cingulum (CING), cingulum–hippocampus tract (CING-Hippo), superior longitudinal fasciculus (SLF) and its temporal cortex branch (SLF-Temp), inferior longitudinal fasciculus, and the inferior fronto-occipital fasciculus (IFOF). For the present study, we did not include forceps minor and forceps major [37,41] because these interhemispheric fibers connect midline structures that are not clearly separable between hemispheres within resting-state ICA component images (left and right posterior cingulate cortices connected by the forceps major and left and right medial frontal cortices connected by the forceps minor). Next, we determined those tracts that could be confirmed to connect DMN brain

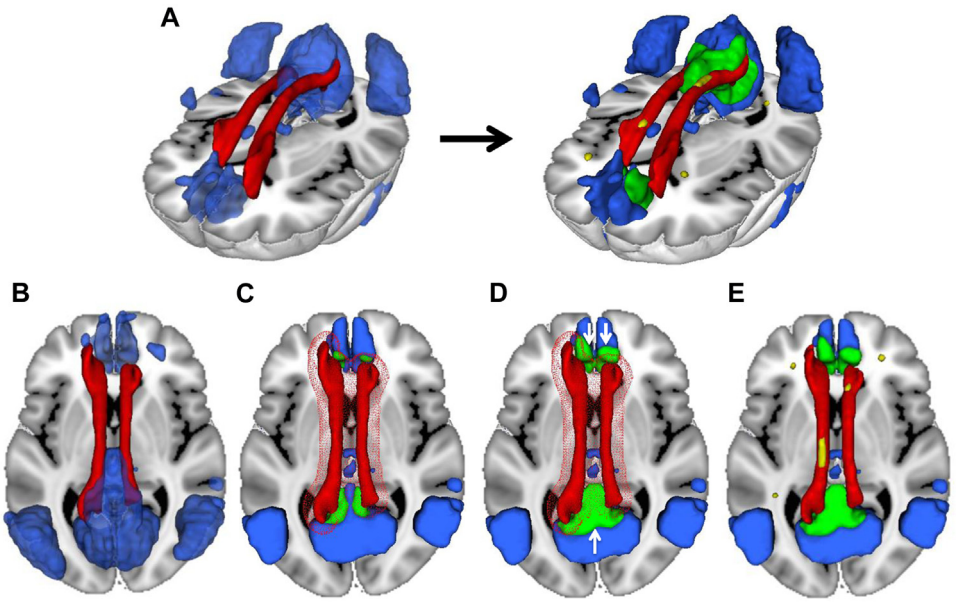

Fig. 1. Schema of successive steps involved in generating the default mode network (DMN) regions of interest (ROI) connected by a tract (here, the cingulum) and the WMH located in that tract. A three-dimensional rendering of the location of the cingulum (red) and the DMN (blue) is shown (A, left panel), where after different processing steps, the final cingulum-connected ROI of the DMN (green) and the WMH (yellow) located in that fiber tract ROI are yielded (A, right panel). (B–E) Illustrate the different processing steps to produce those final ROIs. In the first step, the DMN mask (blue) obtained from a previously published DMN template [27] and the fiber tract mask (red) obtained from the probabilistic JHU fiber tract atlas [32] are fused in MNI space (B). Next, the fiber tract was dilated by 6 mm (meshed red) to determine the area of spatial overlap between the tract and the DMN mask (green, [C]). The green area was dilated in another iteration by 6 mm within the boundaries of the DMN, thus yielding a larger projection area of the fiber tract within the DMN (white arrows pointing to extended green area outside the red meshed sphere, D). This was done to ensure sufficient coverage of the DMN for a representative sampling of DMN FC values within the projection area of the tract. Finally, the spatially normalized WMH map (yellow) was superimposed onto the fiber tract, and the WMH volume within the fiber tract was calculated (E).

regions based on an atlas-based ROI approach. The selected fiber tracts were identified within the probabilistic JHU fiber tract ROI atlas, and the connected brain areas in the DMN were determined as illustrated in Fig. 1. In the first step, a previously published DMN map [27] was binarized at a threshold of $z > 3$, except for the hippocampus region that was thresholded at $z > 2$ to account for typically lower reliability of FC between the hippocampus and other DMN brain regions [42]. The DMN mask was subsequently multiplied by a binary gray matter mask. The gray matter mask was produced by averaging the gray matter probability maps from the SPM-based segmentation (in MNI space) across subjects and thresholding at a gray matter probability score >0.3. The thus produced DMN mask was superimposed onto the JHU fiber tract atlas in MNI space (Fig. 1B). In the second step, the selected tracts in the probabilistic JHU fiber tract atlas [38] were binarized at 10% probability and dilated by 6 mm. The intersection between the dilated fiber tracts and the DMN mask defined then the tract's cortical projection area (Fig. 1C). To provide larger coverage of the projection area within the DMN, the intersecting region was dilated by another 6 mm within the boundaries of the DMN mask, thus yielding the final DMN ROI for a particular tract (Fig. 1D). The ROI was used to extract the mean ROI value from a subject's DMN map for each tract, which was then analyzed in relation to the WMH volume within the same tract (Fig. 1E), calculated as described previously. The maps of all finally selected fiber tract ROIs and associated gray matter ROI are presented in Fig. 2 (see also Supplementary Table 1).

For an additional analysis, the definition of ROIs was repeated using the same procedure, but a DMN template generated from the group ICA within the present study sample was used this time. The maps of all fiber tracts and associated gray matter ROIs resulting from that modified procedure can be found in Supplementary Fig. 3.

2.7. Signal-to-noise ratio of rsfMRI

To control for the variability in fMRI BOLD signal due to field inhomogeneities in T2*-weighted scans [43], we calculated the signal-to-noise ratio (SNR) within each ROI. SNR was defined as the average of the signal intensity across the entire time series divided by the standard deviation of the signal within the time series [43].

2.8. Statistical analysis

For each fiber tract, the ratio between the WMH volume and total white matter volume was calculated (henceforth called WMHr). Normal distribution of gAV-45 PET, WMHr, and FC values was tested in Aβ+ subjects, using

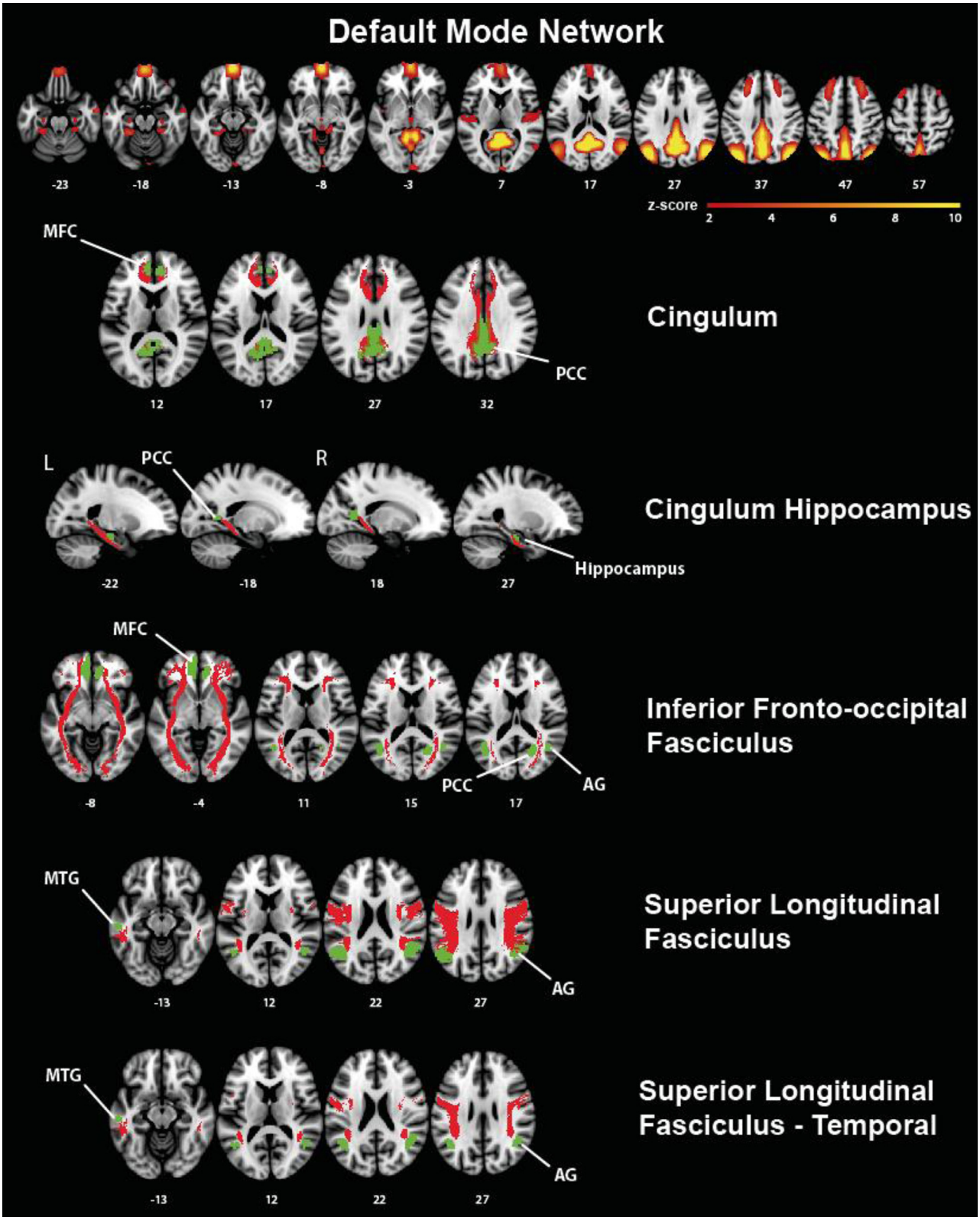

Fig. 2. Major fiber tracts (red) and connected cortical regions of interest (green) of the DMN. The DMN mask was based on the *a priori* DMN map published by Smith et al. [27] as shown in axial view in the upper row. Abbreviations: AG, angular gyrus; L, left; MFC, medial frontal cortex; MTG, middle temporal gyrus; PCC, posterior cingulate cortex; R, right.

Table 1
Group characteristics

	HC Aβ−	HC Aβ+	*P*	MCI Aβ+	*P*	AD	*P*
Sample size	24	14		42		22	
Age (y)*	74.7 (6.6)	74.8 (6.5)	.94	72.4 (6.7)	.19	73.2 (6.9)	.48
Education*	16.0 (2.1)	17.0 (1.9)	.13	16.1 (2.6)	.83	15.7 (2.3)	.72
Gender (F/M)	18/6	6/8	.10	16/26	≤.5	12/10	.25
MMSE*	28.8 (1.3)	28.7 (0.9)	.79	27.3 (1.7)	<.001	22.9 (2.6)	<.001

Abbreviations: Aβ, amyloid-beta; AD, Alzheimer's disease; F, female, HC, healthy controls; M, male; MCI, mild cognitive impairment; MMSE, mini-mental state examination.

*Values indicate the mean (and standard deviation) that is given for each group. *P* values are indicated for differences between HC-Aβ− and each of the other groups based on *t*-tests or chi-square test (gender).

the Shapiro–Wilk test. The WMHr values were not normally distributed ($P < .05$) and were therefore log transformed.

To control for the influence of potentially confounding variables, we tested for each fiber tract if the independent variables WMHr and gAV-45 PET were associated with any of the demographic variables including age, education, or gender. Only the variable "age" showed an association with WMHr ($P < .05$). Therefore, each subject's WMHr score was subsequently adjusted for the influence of age, based on the regression coefficient of age estimated in the HC Aβ− group.

For each fiber tract, nonparametric robust regression analyses (Huber-M) were computed, with FC within the tract's gray matter ROI as the dependent variable. The independent variables included WMHr, gAV-45 PET, diagnosis (HC Aβ+, MCI Aβ+, and AD dementia), and SNR (within the connected ROI). We controlled for SNR because rsfMRI scans showed in most cases pencil-shaped patterns of SNR. Gender was included as an additional variable due to numerical (although not significant) difference between diagnostic groups. Improvements in model fit by adding two-way interaction terms of diagnosis × WMHr or WMHr × AV-45 PET were tested. The normal distribution of the residuals was examined for each significant regression model, using the Shapiro–Wilk test. The significance threshold was $\alpha < 0.05$ (one-tailed) for testing our directional hypotheses of the effect of WMHr and gAV-45 PET on FC. To test the robustness of findings, we bootstrapped the regression analysis, with the coefficient of WMHr and AV-45 PET being estimated in N = 999 bootstrap iterations. We report the mean bootstrapped beta coefficient and the 95% confidence interval (95% CI).

Voxel-based lesion probability mapping of WMH was done based on the binarized WMH maps within the entire sample (AD dementia, MCI Aβ+, and HC Aβ+) [44]. All statistical analyses were done with the software library R.

3. Results

Table 1 summarizes the demographic characteristics for each diagnostic group. Supplementary Table 2 summarizes the mean values of WMHr, ROI-FC, and gAV-45 PET.

3.1. Association between WMHr and FC

Greater WMHr within the IFOF was associated with reduced FC of the IFOF-connected gray matter ROIs, independently of gAV-45 PET levels ($\beta = -5.6$, $t(72) = -2.051$, $P = .02$, Fig. 3). Bootstrapping of the regression analysis confirmed the association between IFOF WMHr and lower FC (bootstrapped $\beta = -6.6$, 95% CI = −14.2 to −1.2). None of the other fiber tracts demonstrated a main effect of WMHr. None of the two-way interactions (WMHr × diagnosis or WMHr × gAV-45 PET) were significant, with outliers excluded (Supplementary Table 3). In addition, we tested whether GM volume within each fiber tracts' connected brain area is a confounding factor. However, no associations between GM volume and WMHr for any of the fiber

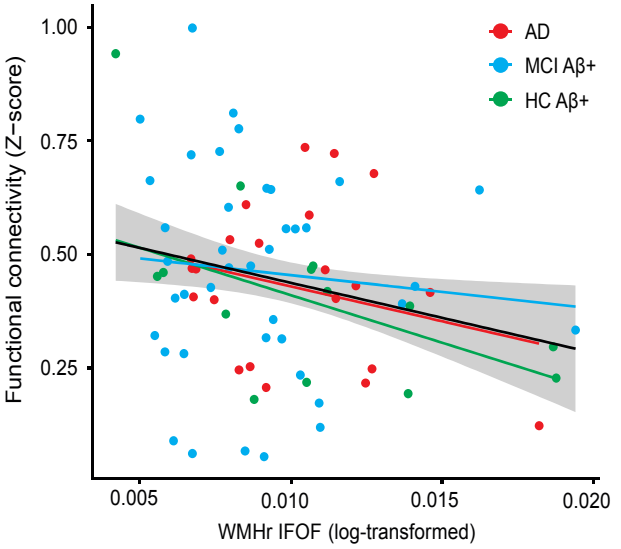

Fig. 3. Regression plots showing functional connectivity in the inferior fronto-occipital fasciculus (IFOF)–connected regions of interest of the DMN as a function of WMHr in the IFOF. The regression lines for each group (colored) and the whole sample (solid black line) and the standard error of the estimate (shaded area) are shown. Higher WMHr in the IFOF was associated with lower FC in the gray matter projection area of the IFOF. Statistical outliers (>3 standard deviation from group mean) have been removed for purposes of the current graph (robust regression model accounted for outliers in the regression analysis). Abbreviation: WMHr, ratio between the WMH volume and total white matter.

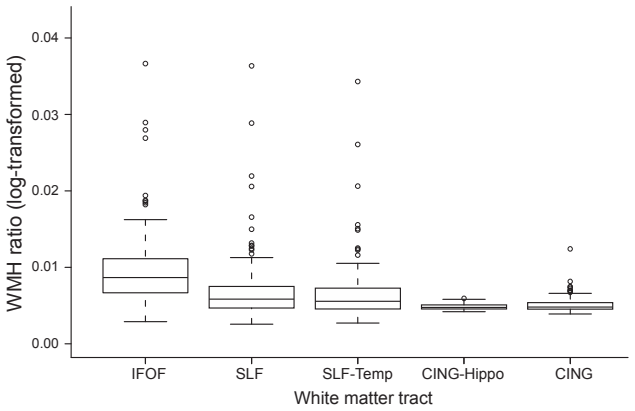

Fig. 4. The box-whisker plot of WMHr in each selected fiber tract region of interest. Statistical outliers are shown as circles. The IFOF showed a significantly higher WMHr compared with each of the other fiber tract regions of interest. Abbreviations: IFOF, inferior fronto-occipital fasciculus; WMHr, ratio between the WMH volume and total white matter.

tract ROIs were found ($P > .05$). Stepwise forward regression showed that both IFOF-ROI GM volume and IFOF WMHr independently predicted FC. The association between higher WMHr in the IFOF and lower FC in connected brain areas of the DMN was confirmed ($\beta = -9.0$, $t(72) = -2.3802$, $P = .01$, Supplementary Fig. 4), when spatially defining the DMN regions by the group-specific DMN map rather than the *a priori* selected DMN mask [27]. None of the two-way interactions (WMHr × diagnosis or WMHr × gAV-45 PET) were significant. To test whether global WMHr (excluding WMHr of the IFOF) added to the prediction of FC changes, we added both IFOF-WMHr and global WMHr (excluding WMHr of the IFOF) in a stepwise forward regression model, controlled for age, gender, education, and diagnosis. Results showed that only WMHr of the IFOF was predictive of FC ($\beta = -6.26$, $t = -2.312$, $P = .012$).

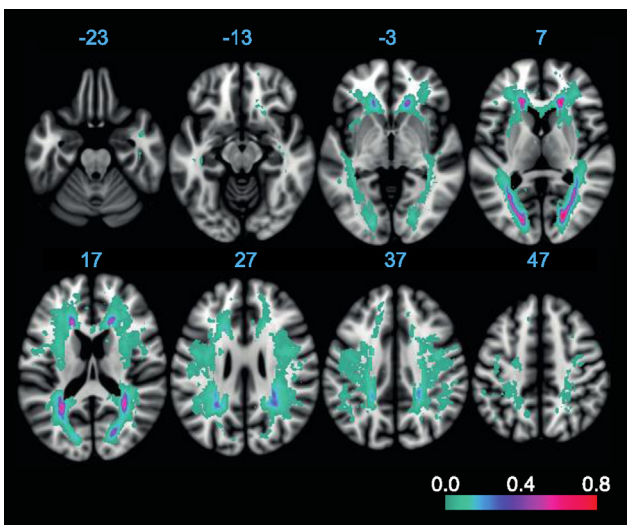

Fig. 5. Lesion probability map of WMH including the voxel-wise mapping of the proportion of subjects showing a WMH in a particular voxel. The proportion of WMH occurrence is color-coded in each voxel, with low values shown in green–blue colors and high values in red colors.

3.2. Distribution of WMH within the DMN tracts

Next, we investigated whether WMHr differed between fiber tracts of the DMN or whether WMHs were rather homogenously distributed within the DMN. Fig. 4 shows the mean WMHr for each fiber tract. WMHr within the IFOF was significantly higher compared with each of the other tracts ($F(4,73) = 111.8$, $P < .001$; see also Supplementary Table 2). WMH probability mapping showed that WMHs were predominantly distributed around posterior and anterior periventricular regions (Fig. 5), which include pathways of the IFOF and SLF tracts within the DMN.

3.3. Association between global AV-45 PET binding and FC

Greater gAV-45 PET binding was associated with lower ROI-FC values in the projection brain areas of the IFOF ($t(72) = -1.81$, $P = .037$), CING-Hippo ($t(72) = -1.93$, $P = .029$), and at trend level for the SLFtemp ($\beta = -0.15$, $t = -1.4$, $P = .08$). Bootstrapping of the regression coefficient of AV-45 PET confirmed a significant effect for the IFOF ($\beta = -0.28$, 95% CI = −0.55 to −0.004) and a trend for the CING-Hippo ($\beta = -0.75$, 95% CI = 0.007 to −1.5). Regression plots are presented in Fig. 6. None of the WMHr measures were associated with gAV-45 PET binding.

3.4. Association between WMHr and other resting-state networks

To test whether the current results on the association between WMHr and AV-45 PET with FC were specific for the DMN, we tested the association between those predictors and FC changes in two control rsfMRI networks, including the auditory network and the dorsal attentional network maps [27]. Because none of the atlas-based fiber tract ROIs of the DMN-connected regions of those two resting-state networks, we did not expect any correlation between WMHr and FC for those networks. Applying the same spatial ROIs and using the same regression models, we did not find any association between WMHr and FC for any of the fiber tract ROIs.

4. Discussion

The major findings of the present study are that: (1) the IFOF showed the highest WMHr among all atlas-based fiber tract ROIs of the DMN, (2) WMHr in the fiber tract ROI of the IFOF was associated with reduced FC in the connected brain regions, (3) the association between higher WMHr and lower FC was independent of gAV45 PET, and (4) higher gAV45 PET was independently associated with reduced FC within DMN areas. These results suggest that WMHr disrupt FC in a fiber tract–specific way and

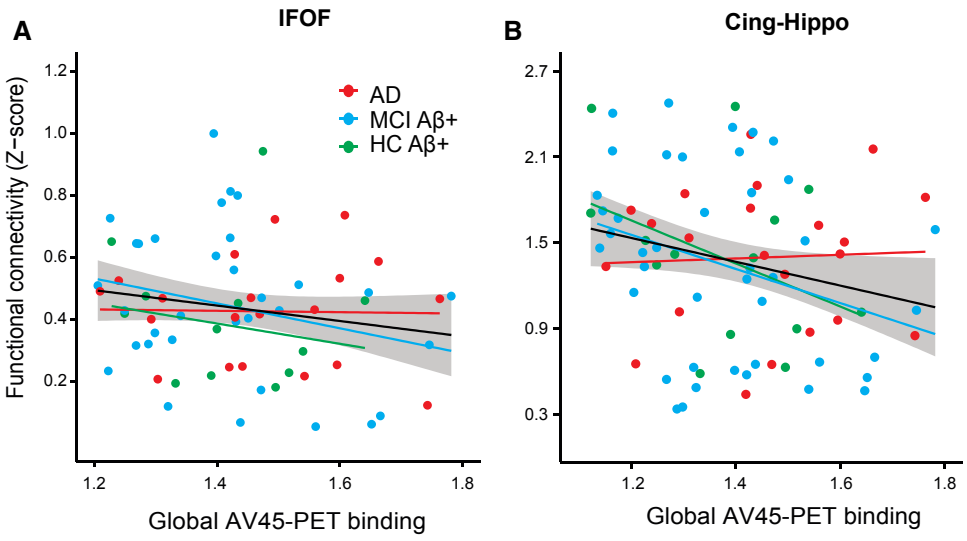

Fig. 6. Regression plots showing functional connectivity (FC) in gray matter ROIs as a function of levels of gAV-45 PET. The regression lines for each group (colored) and the whole sample (solid black line) and the standard error of the estimate (shaded area) are shown. Higher global AV-45 PET was associated with lower FC in the gray matter regions of interest connected by the IFOF (A) and hippocampus–cingulum tract (B). Statistical outliers (>3 standard deviation from group mean) have been removed for purposes of the current graph (robust regression model accounted for outliers in the statistical analysis). Abbreviation: IFOF, inferior fronto-occipital fasciculus.

contribute independently from Aß pathology to reduced FC within the DMN.

The IFOF showed a particularly high WMHr when compared with other fiber tracts of the DMN. The IFOF is a long association tract that passes through the periventricular white matter [45], that is, the sparsely perfused vascular end zone of perforating arteries [46]. Sparse perfusion of the IFOF may thus explain the high WMH volume of that tract. The current results of selective effects for the IFOF suggest that only at a sufficiently high severity level, WMH volume disrupts FC. Although the interpretation in favor of a threshold effect is tempting, we caution that any smaller effects of WMH in tracts other than the IFOF may have not been detected due to lower statistical power. Thus, the threshold hypothesis of the effect of WMH on FC awaits further confirmation.

We found effects of WMH onto FC to be additive to those observed for gAV-45 PET, and no interaction with gAV-45 PET was observed. These results are in keeping with previous studies reporting additive rather than synergistic effects of WMH and global Aβ levels on FDG-PET and cognitive function in AD [47]. Moreover, the levels of gAV45 PET were not associated with WMHr in any of the fiber tracts of the DMN, consistent with previous studies that found no association between global levels of WMH and global levels of Aβ [2,48]. Together, these results suggest that WMH and Aβ pathology contribute independently to functional changes within the DMN. Still, the absence of an interaction effect reported in many neuroimaging studies should be cautiously interpreted with regard to conclusions about the association between vascular pathology and Aβ deposition. WMHs are a radiological surrogate measure of white matter changes of presumed vascular origin, where the sensitivity to detect underlying vascular pathology is unclear [49]. Given that many risk factors of AD such as high blood pressure, hyperlipidemia, or diabetes are associated with vascular pathology [50–52], it remains to be clarified whether vascular pathology and primary AD pathology such as Aβ are truly independent disease processes.

There are several caveats that need to be taken into account when interpreting our results.

First, we did not assess fiber tract connections via diffusion tensor imaging directly but applied an atlas-based fiber tract ROI approach. Although this approach has the advantage of avoiding problems of fiber tracking such as failure due to white matter lesions, the current approach cannot assure that fiber tracts always connected the DMN brain regions. Based on the group ICA map of the DMN, we observed for the SLF fiber tract ROIs a connection to the angular gyrus but not the middle temporal gyrus (Supplementary Fig. 3), which may explain why we did not find an association between WMHr in the SLF and DMN brain regions.

Second, we included only subjects with abnormally increased levels of Aß. Hence, the observed association between WMH and reduced FC may not necessarily be generalizable to subjects with low levels of Aβ. However, because Aβ levels are associated with abnormal FC in the DMN particularly at pathologically increased but not low levels of Aβ [53], we specifically chose the present study design for a rigorous test of our hypothesis that WMHs, in addition to Aβ pathology, contribute to changes in the DMN.

Third, we used only global levels of AV-45 PET binding rather than levels of Aβ in the DMN as a predictor of FC changes. We chose the global measure of Aβ level because in subjects with abnormally increased levels of Aβ, the PET levels of Aβ binding are highly correlated between different cortical brain areas. Thus, the average cortical AV-45 PET binding can be considered a valid estimate of the level of Aβ deposition within the DMN.

Fourth, the AV-45 PET scans were acquired sometimes months apart from the rsfMRI scan. Previous longitudinal studies have shown a 1% to 2% annual change in global AV-45 PET binding [54] with rather subtle spatial expansion [55]. This variability may have limited the power to detect an association between AV-45 PET and FC changes in the present study.

Lastly, we focused on the DMN rather than other resting-state networks. We specifically chose the DMN because this resting-state network is predominantly affected in AD. Our results provide evidence that even in a resting-state network where Aβ accumulation is high and Aβ is associated with reduced FC, increased WMHs still add to reduced FC in that network in AD. However, other resting-state networks such as the fronto-parietal attention network [56] may be affected by WMH in AD as well [57].

In conclusion, the current results support the notion of localized effects of WMH on the functional integrity of the DMN. These effects of WMH were independent from the effects of global levels of Aβ, suggesting a linear additive contribution of both cerebrovascular-related fiber tract impairment and Aβ pathology to functional network alterations. For vascular brain changes, treatment options and preventative interventions are already available. The current approach offers a promising way to pinpoint the effects of cerebrovascular pathology–related impairment of functional networks and thus to potentially serve as an outcome parameter for clinical trials.

Acknowledgments

Data used in preparation of this article were obtained from the Alzheimer's Disease Neuroimaging Initiative (ADNI) database (adni.loni.ucla.edu). As such, the investigators within the ADNI contributed to the design and implementation of ADNI and/or provided data but did not participate in analysis or writing of this report. A complete listing of ADNI investigators can be found in "Additional Authors" supplemental material and at http://adni.loni.ucla.edu/wpcontent/uploads/how_to_apply/ADNI_Acknowledgement_List.pdf. This work was supported by grants of the LMUexcellent Initiative (ADDMe), Alzheimer's Forschung Initiative (AFI) and the European Commission (PCIG12-GA-2012-334259, VASCAMY) to M.E.; the Vascular Dementia Research Foundation to Martin Dichgans; Merck, Avid, the Veterans Administration (VA) and Department of Defense (DOD) to M.W.W.; grant numbers 2U01AG024904, W81XWH-13-1-0259, W81XWH-12-2-0012, R01 AG10897, 1P41 EB015904, P01 AG19724, R01 AG032306, R01A G03879, ADNI 2-12-233036, 20110506, R01 MH098062-01 from the following sources: National Institutes of Health/National Institutes Alzheimer's/National Institute of Mental Health, Department of Defense, gs12:Alzheimer's Association, gs13:Alzheimer's Drug Discovery Foundation, to M.W.W.; travel expenses for lectures from the United Leukodystrophy Foundation, the European Stroke Conference, and Kenes International to M.D.

Supplementary data

Supplementary data related to this article can be found at http://dx.doi.org/10.1016/j.jalz.2016.06.2358.

RESEARCH IN CONTEXT

1. Systematic review: Global levels of white matter hyperintensities (WMHs) were associated with reduced brain function (FDG-PET or fMRI; [4]; [10]) and added to the effects of increased Aß in AD ([8]). Which functional networks show reduced integrity in association with WMH is debated. WMHs are heterogeneously distributed in the WM and may affect the gray matter in a fiber tract–specific way (Duering et al., 2014, Reference 33).
2. Interpretation: Higher tract-based WMH and lower FC were associated selectively in brain areas connected by the IFOF, that is, the fiber tract showing the highest WMH among all tracts of the DMN. These results suggest that WMH are associated with reduced FC in a tract-specific way rather than global way, independently of Aß.
3. Future direction: Are WMHs in particular fiber tracts associated with altered memory task–related activation and thus may contribute to cognitive impairment in Alzheimer's disease?

References

[1] Debette S, Markus HS. The clinical importance of white matter hyperintensities on brain magnetic resonance imaging: systematic review and meta-analysis. BMJ 2010;341:c3666.
[2] Marchant NL, Reed BR, DeCarli CS, Madison CM, Weiner MW, Chui HC, et al. Cerebrovascular disease, beta-amyloid, and cognition in aging. Neurobiol Aging 2012;33:e25–36.
[3] Kochunov P, Ramage AE, Lancaster JL, Robin DA, Narayana S, Coyle T, et al. Loss of cerebral white matter structural integrity tracks the gray matter metabolic decline in normal aging. Neuroimage 2009;45:17–28.

[4] Lo RY, Jagust WJ, Alzheimer's Disease Neuroimaging Initiative. Vascular burden and Alzheimer disease pathologic progression. Neurology 2012;79:1349–55.
[5] Reed BR, Eberling JL, Mungas D, Weiner M, Kramer JH, Jagust WJ. Effects of white matter lesions and lacunes on cortical function. Arch Neurol 2004;61:1545–50.
[6] DeCarli C, Murphy D, Tranh M, Grady C, Haxby J, Gillette J, et al. The effect of white matter hyperintensity volume on brain structure, cognitive performance, and cerebral metabolism of glucose in 51 healthy adults. Neurology 1995;45:2077–84.
[7] Tullberg M, Fletcher E, DeCarli C, Mungas D, Reed B, Harvey D, et al. White matter lesions impair frontal lobe function regardless of their location. Neurology 2004;63:246–53.
[8] Haight TJ, Landau SM, Carmichael O, Schwarz C, DeCarli C, Jagust WJ, et al. Dissociable effects of Alzheimer disease and white matter hyperintensities on brain metabolism. JAMA Neurol 2013; 70:1039–45.
[9] Kuczynski B, Reed B, Mungas D, Weiner M, Chui HC, Jagust W. Cognitive and anatomic contributions of metabolic decline in Alzheimer disease and cerebrovascular disease. Arch Neurol 2008; 65:650–5.
[10] Zhou Y, Yu F, Duong TQ, for the Alzheimer's Disease Neuroimaging Initiative. White matter lesion load is associated with resting state functional MRI activity and amyloid pet but not FDG in mild cognitive impairment and early alzheimer's disease patients. J Magn Reson Imaging 2015;41:102–9.
[11] Tullberg M, Fletcher E, DeCarli C, Mungas D, Reed BR, Harvey DJ, et al. White matter lesions impair frontal lobe function regardless of their location. Neurology 2004;63:246–53.
[12] Biesbroek JM, Kuijf HJ, van der Graaf Y, Vincken KL, Postma A, Mali WP, et al. Association between subcortical vascular lesion location and cognition: a voxel-based and tract-based lesion-symptom mapping study. The SMART-MR study. PLoS One 2013; 8:e60541.
[13] DeCarli C, Fletcher E, Ramey V, Harvey D, Jagust WJ. Anatomical mapping of white matter hyperintensities (WMH): exploring the relationships between periventricular WMH, deep WMH, and total WMH burden. Stroke 2005;36:50–5.
[14] Duering M, Zieren N, Herve D, Jouvent E, Reyes S, Peters N, et al. Strategic role of frontal white matter tracts in vascular cognitive impairment: a voxel-based lesion-symptom mapping study in CADASIL. Brain 2011;134:2366–75.
[15] Duering M, Righart R, Csanadi E, Jouvent E, Herve D, Chabriat H, et al. Incident subcortical infarcts induce focal thinning in connected cortical regions. Neurology 2012;79:2025–8.
[16] Koch W, Teipel S, Mueller S, Buerger K, Bokde AL, Hampel H, et al. Effects of aging on default mode network activity in resting state fMRI: does the method of analysis matter? Neuroimage 2010; 51:280–7.
[17] Koch K, Myers NE, Gottler J, Pasquini L, Grimmer T, Forster S, et al. Disrupted intrinsic networks link amyloid-beta pathology and impaired cognition in prodromal Alzheimer's disease. Cereb Cortex 2015;25:4678–88.
[18] Sperling RA, Laviolette PS, O'Keefe K, O'Brien J, Rentz DM, Pihlajamaki M, et al. Amyloid deposition is associated with impaired default network function in older persons without dementia. Neuron 2009;63:178–88.
[19] Mueller SG, Weiner MW, Thal LJ, Petersen RC, Jack CR, Jagust W, et al. Ways toward an early diagnosis in Alzheimer's disease: The Alzheimer's Disease Neuroimaging Initiative (ADNI). Alzheimers Dement 2005;1:55–66.
[20] McKhann G, Drachman D, Folstein M, Katzman R, Price D, Stadlan EM. Clinical diagnosis of Alzheimer's disease: report of the NINCDS-ADRDA Work Group under the auspices of Department of Health and Human Services Task Force on Alzheimer's Disease. Neurology 1984;34:939–44.
[21] Petersen RC, Aisen PS, Beckett LA, Donohue MC, Gamst AC, Harvey DJ, et al. Alzheimer's Disease Neuroimaging Initiative (ADNI): clinical characterization. Neurology 2010;74:201–9.
[22] Petersen RC, Smith GE, Waring SC, Ivnik RJ, Tangalos EG, Kokmen E. Mild cognitive impairment: clinical characterization and outcome. Arch Neurol 1999;56:303–8.
[23] Landau SM, Breault C, Joshi AD, Pontecorvo M, Mathis CA, Jagust WJ, et al. Amyloid-β imaging with Pittsburgh compound B and florbetapir: comparing radiotracers and quantification methods. J Nucl Med 2013;54:70–7.
[24] Ashburner J. A fast diffeomorphic image registration algorithm. Neuroimage 2007;38:95–113.
[25] Song XW, Dong ZY, Long XY, Li SF, Zuo XN, Zhu CZ, et al. REST: a toolkit for resting-state functional magnetic resonance imaging data processing. PLoS One 2011;6:e25031.
[26] Calhoun VD, Adali T, Pearlson GD, Pekar JJ. A method for making group inferences from functional MRI data using independent component analysis. Hum Brain Mapp 2001;14:140–51.
[27] Smith SM, Fox PT, Miller KL, Glahn DC, Fox PM, Mackay CE, et al. Correspondence of the brain's functional architecture during activation and rest. Proc Natl Acad Sci U S A 2009;106:13040–5.
[28] Zhang Y, Brady M, Smith S. Segmentation of brain MR images through a hidden Markov random field model and the expectation-maximization algorithm. IEEE Trans Med Imaging 2001;20:45–57.
[29] Smith SM, Jenkinson M, Woolrich MW, Beckmann CF, Behrens TE, Johansen-Berg H, et al. Advances in functional and structural MR image analysis and implementation as FSL. Neuroimage 2004;23 Suppl 1:S208–19.
[30] Otsu N. A thresholding selection method from gray-level histogram. IEEE Trans Syst Man Cybern 1979;9:62–6.
[31] Jenkinson M, Bannister P, Brady M, Smith S. Improved optimization for the robust and accurate linear registration and motion correction of brain images. Neuroimage 2002;17:825–41.
[32] Hua K, Zhang J, Wakana S, Jiang H, Li X, Reich DS, et al. Tract probability maps in stereotaxic spaces: analyses of white matter anatomy and tract-specific quantification. Neuroimage 2008;39:336–47.
[33] Duering M, Gesierich B, Seiler S, Pirpamer L, Gonik M, Hofer E, et al. Strategic white matter tracts for processing speed deficits in age-related small vessel disease. Neurology 2014;82:1946–50.
[34] Damoiseaux JS, Greicius MD. Greater than the sum of its parts: a review of studies combining structural connectivity and resting-state functional connectivity. Brain Struct Funct 2009;213:525–33.
[35] Horn A, Ostwald D, Reisert M, Blankenburg F. The structural-functional connectome and the default mode network of the human brain. Neuroimage 2014;102 Pt 1:142–51.
[36] Greicius MD, Supekar K, Menon V, Dougherty RF. Resting-state functional connectivity reflects structural connectivity in the default mode network. Cereb Cortex 2009;19:72–8.
[37] Huang S, Yeh F, Chang W, Lin F, Tseng W. Connective fiber tracts in default mode network mapped by resting state fMRI and diffusion spectrum imaging. Proc Intl Soc Mag Reson Med 2009:648.
[38] Teipel SJ, Bokde AL, Meindl T, Amaro E Jr, Soldner J, Reiser MF, et al. White matter microstructure underlying default mode network connectivity in the human brain. Neuroimage 2010;49:2021–32.
[39] van den Heuvel MP, Mandl RC, Kahn RS, Hulshoff Pol HE. Functionally linked resting-state networks reflect the underlying structural connectivity architecture of the human brain. Hum Brain Mapp 2009; 30:3127–41.
[40] van den Heuvel M, Mandl R, Luigjes J, Hulshoff Pol H. Microstructural organization of the cingulum tract and the level of default mode functional connectivity. J Neurosci 2008;28:10844–51.
[41] van den Heuvel MP, Mandl RC, Kahn RS, Hulshoff Pol HE. Functionally linked resting-state networks reflect the underlying structural connectivity architecture of the human brain. Hum Brain Mapp 2009; 30:3127–41.

[42] Mueller S, Wang D, Fox MD, Pan R, Lu J, Li K, et al. Reliability correction for functional connectivity: theory and implementation. Hum Brain Mapp 2015;36:4664–80.
[43] Yeo BT, Krienen FM, Sepulcre J, Sabuncu MR, Lashkari D, Hollinshead M, et al. The organization of the human cerebral cortex estimated by intrinsic functional connectivity. J Neurophysiol 2011; 106:1125–65.
[44] Rorden C, Karnath H, Bonilha L. Improving lesion-symptom mapping. J Cogn Neurosci 2007;19:1081–8.
[45] Wakana S, Jiang H, Nagae-Poetscher LM, van Zijl PC, Mori S. Fiber tract-based atlas of human white matter anatomy. Radiology 2004; 230:77–87.
[46] Holland CM, Smith EE, Csapo I, Gurol ME, Brylka DA, Killiany RJ, et al. Spatial distribution of white-matter hyperintensities in Alzheimer disease, cerebral amyloid angiopathy, and healthy aging. Stroke 2008; 39:1127–33.
[47] Ortner M, Kurz A, Alexopoulos P, Auer F, Diehl-Schmid J, Drzezga A, et al. Small vessel disease, but neither amyloid load nor metabolic deficit, is dependent on age at onset in Alzheimer's disease. Biol Psychiatry 2015;77:704–10.
[48] Grimmer T, Faust M, Auer F, Alexopoulos P, Förstl H, Henriksen G, et al. White matter hyperintensities predict amyloid increase in Alzheimer's disease. Neurobiol Aging 2012;33:2766–73.
[49] Wardlaw JM, Smith EE, Biessels GJ, Cordonnier C, Fazekas F, Frayne R, et al. Neuroimaging standards for research into small vessel disease and its contribution to ageing and neurodegeneration. Lancet Neurol 2013;12:822–38.
[50] O'Brien JT, Markus HS. Vascular risk factors and Alzheimer's disease. BMC Med 2014;12:218.
[51] Breteler MM. Vascular risk factors for Alzheimer's disease: an epidemiologic perspective. Neurobiol Aging 2000;21:153–60.
[52] Dichgans M, Zietemann V. Prevention of vascular cognitive impairment. Stroke 2012;43:3137–46.
[53] Lim HK, Nebes R, Snitz B, Cohen A, Mathis C, Price J, et al. Regional amyloid burden and intrinsic connectivity networks in cognitively normal elderly subjects. Brain 2014;137:3327–38.
[54] Landau SM, Fero A, Baker SL, Koeppe R, Mintun M, Chen K, et al. Measurement of longitudinal beta-amyloid change with 18F-florbetapir PET and standardized uptake value ratios. J Nucl Med 2015;56:567–74.
[55] Forster S, Grimmer T, Miederer I, Henriksen G, Yousefi BH, Graner P, et al. Regional expansion of hypometabolism in Alzheimer's disease follows amyloid deposition with temporal delay. Biol Psychiatry 2012;71:792–7.
[56] Damoiseaux JS, Rombouts SA, Barkhof F, Scheltens P, Stam CJ, Smith SM, et al. Consistent resting-state networks across healthy subjects. Proc Natl Acad Sci U S A 2006;103:13848–53.
[57] Jacobs HI, Visser PJ, Van Boxtel MP, Frisoni GB, Tsolaki M, Papapostolou P, et al. Association between white matter hyperintensities and executive decline in mild cognitive impairment is network dependent. Neurobiol Aging 2012;33:e1–8.